Journal of Engineering Mathematics **40:** 43–58, 2001.

On the initial stages of cement hydration

S. J. PREECE, J. BILLINGHAM and A. C. KING
School of Mathematics and Statistics, University of Birmingham, Edgbaston, Birmingham B15 2TT, United Kingdom

Received 21 May 1999; accepted in revised form 23 March 2000

Abstract. After the initial mixing of cement, an induction period occurs during which its consistency remains constant. Thickening occurs at the end of this period when the consistency is observed to increase very rapidly. In this paper we propose a reaction-diffusion model for the hydration of tricalcium silicate, a principal constituent of cement, which is believed to be responsible for the initial development of its strength. Our model is based on the assumption that the hydration of cement can be described as a dissolution -precipitation reaction. The mathematical solutions enable us to determine some of the factors that control the length of the induction period and make predictions of the ionic concentrations which are in agreement with experimental data.

Key words: cement hydration, tricalcium silicate, induction period, reaction-diffusion, mathematical modelling.

1. Introduction

Although it is primarily used in the construction industry, cement is of vital importance during the construction of oilwells. Once the drilling of an oilwell is complete, a steel casing is inserted into the borehole and fixed in place by cement. The cement slurry is pumped down the well bore and rises up from the well base in the annular region between the rock and the outer casing. The slurry must stay pumpable for sufficient time to permit placement under given well conditions and it is thus essential that the thickening time of the cement can be predicted accurately.

On mixing with water, an induction period occurs during which the consistency of the cement remains constant. Thickening occurs at the end of this period, when the consistency is observed to increase very rapidly. It has been argued [1], [2], [3] that much of the heat evolved during the initial stages of hydration can be attributed to the hydration of one of the principal components of cement, tricalcium silicate. It would therefore seem that an understanding of the induction period can be gained by studying this simpler hydration reaction. In this paper we adopt this viewpoint and propose a reaction-diffusion model for the hydration of tricalcium silicate (C_3S). We note that cement chemistry nomenclature is used throughout this paper in which the following abbreviations are adopted: $C = CaO$, $S = SiO_2$ and $H = H_2O$.

The two hydration products of C_3S are hydrated calcium silicate (C-S-H) and calcium hydroxide (CH). On contact with water, ions are liberated from the C_3S and a very thin layer of C-S-H forms on the surface of each of the grains. The structural evolution from then on is the subject of much debate, but the thickening of the cement is believed to occur after the induction period when a secondary growth of C-S-H causes hydration shells from adjacent grains to coalesce and the cement to thicken.

In general terms, theories that attempt to explain the hydration mechanism fall into two categories: protective coating theories and delayed nucleation theories. Of the protective coat-

ing theories there are two main schools of thought. The first is based on the observation that C-S-H occurs in a number of morphological forms and was first proposed by Stein and Stevels [4]. The different types of C-S-H have different permeabilities, and hence act to control the rate at which the hydration of the cement grains proceeds. A mechanism was suggested by De Jong et al. [5] in which the C-S-H undergoes three phase transformations during the induction period. With each transformation it becomes increasingly permeable, which leads to more rapid hydration of the initial grain of C_3S. The rate of transition between the three different types of C-S-H was predicted to be dependent on the level of calcium hydroxide in solution. The second protective coating theory is known as the osmotic pressure hypothesis and was first proposed by Powers [6]. Although it has been favoured over the last few decades [1], [7], [8], [9] in recent years it has received less attention. On contact with water a thin hydration shell is again assumed to form at the surface of the grain. Because of their relative size, water and calcium ions, but not silica ions, can diffuse through this shell. As this process continues an osmotic pressure builds up because the silica ions cannot escape. The end of the induction period is marked by the rupture of the shell by osmotic pressure and the formation of the secondary C-S-H.

The second proposed mechanism involves a delay in the build up of C-S-H, which corresponds to the observed induction period. There are many possible mechanisms that could control the growth of C-S-H. One theory, put forward by Lota et al. [10], is that the growth of C-S-H on the surface of the grain is dependent on the concentration of calcium ions in solution. At the end of the induction period the solution becomes supersaturated with respect to calcium hydroxide, which then precipitates. This increases the rate of formation of C-S-H and the cement begins to thicken. This view is supported by Damidot and Nonat [11] who also argue that it is the concentration of calcium ions in solution which is the most important factor in governing tricalcium silicate hydration.

A few authors have attempted to model the hydration of cement and tricalcium silicate. Bentz et al. [12] studied the microstructural development during cement hydration using cellular automaton techniques. This simulation was initiated using a digital image of a real suspension of cement in water. The microstructural development was then modelled by allowing dissolution, mass transport and chemical reaction to occur on a lattice which was assumed to be small enough to capture mass transport effectively. They assumed that the cement formed its hydration products on contact with water and that these hydration products diffused and subsequently nucleated in the pore solution. The images generated seem to agree well with real cement samples. A similar model has been proposed by Tzschichholz et al. [13] in which mass is transported by the diffusion of ions, whilst the hydrated phases are assumed to be immobile. This simulation began with real initial configurations of anhydrous cement particles and was able to reproduce qualitatively the basic features of cement hydration. Although this type of model successfully displays the effect of different variables on the degree of hydration required for the cement to set, it is not possible to use it to obtain an exact functional relation between thickening time and the measurable properties of cement.

Conceptual models for the hydration of tricalcium silicate have been developed by Kondo and Ueda [14] and Pommersheim et al. [15, 16]. Pommersheim et al. considered a spherically-symmetric grain of tricalcium silicate. They assumed a three layer structure in which the grain recedes away from its original boundary. At this original boundary they postulated the existence of a middle or barrier layer. Outside this barrier is an outer hydration product and inside, an inner hydration product. They assumed that soluble hydrates are produced in the reaction between water and tricalcium silicate and that these hydrates diffuse outwards and precipitate

at some point within the three layer structure. They further assumed that the diffusivity of the chemical species is different in each of the layers and were able to predict the degree of hydration of the grain with time. Although conceptual models give a description of the microstructural evolution of a grain of tricalcium silicate based on experimental ideas, they lack fundamental chemistry. Because of this it is not possible to use these models to make predictions about the nature of cement hydration. The models discussed also make no attempt to determine the factors that control the thickening time of cement.

The model proposed in this paper is based on the observation [11], [17] that the hydration of cement can be described as a dissolution-precipitation mechanism. The fundamental laws of mass transport and basic cement reaction kinetics are used to construct a reaction-diffusion model of the hydration of tricalcium silicate. By analysing the model we are able to determine the factors that control the length of the induction period and thus the thickening time of cement. We can also make predictions of the behaviour of the ionic concentrations, which agree with experimental observations.

2. The chemistry of tricalcium silicate hydration

On contact with water, tricalcium silicate dissolves to produce calcium, hydroxide and silica ions. In this paper we follow the example of Tzschichholz et al. [13] who assumed that ions are transported in the pore solution by diffusion, and recombine in solution to form immobile hydration products. Experimental tests carried out by Rugby Cement have shown that, even when the temperature of the hydration reaction is kept constant, variation in the thickening times between different cement samples is commonly observed. We thus consider an isothermal hydration reaction. The reaction between water and C_3S is a surface reaction that can be described by the equation [11]

$$C_3S + 3H_2O \rightarrow 3Ca^{2+} + 4OH^- + H_2SiO_4^{2-}, \quad \text{rate} \quad Q_1, \tag{1}$$

where $H_2SiO_4^{2-}$ denotes a silica ion. In the first part of this paper we assume that this reaction proceeds at a constant rate and for mathematical convenience define the constant k_1 such that $Q_1 = 8k_1$. The constant k_1 is the flux of each ion into solution from the surface of the grain and has units of mol m^{-2} s^{-1}. In Section 6 we modify the reaction rate to describe a decrease in ion flux as the hydration products build up.

Once produced, the ions diffuse into the surrounding solution and the ionic concentrations begin to increase. The insoluble hydration products then precipitate out of solution. To avoid complication, we make the same assumption as Tzschichholz et al. [13] and consider only one stoichiometric form of C-S-H. Although this may seem to be an oversimplification the results of the model are found to be unaffected qualitatively if the factor of 1·5 in Equation (2) is varied between 1 and 3. Experimental measurements show all values of the factor to lie within this range. The formation of the hydration products from the ions is described by the reactions [11]

$$H_2SiO_4^{2-} + 1{\cdot}5Ca^{2+} + OH^- + H_2O \rightarrow \text{C-S-H}, \quad \text{rate} \quad Q_2, \tag{2}$$

$$Ca^{2+} + 2OH^- \rightarrow CH. \tag{3}$$

The C-S-H is always first to precipitate, and it has been suggested [18], [19], [20] that precipitation occurs once the solubility product,

$$S = [Ca^{2+}]^{1.5}[OH^-][H_2SiO_4^{2-}], \tag{4}$$

reaches a critical equilibrium value, S_{eq}. Above this threshold it is assumed that precipitation occurs at a constant rate. As reaction (2) proceeds C-S-H build up in solution. This build up has been described as a polymerisation reaction [10]. The polymerisation cannot continue indefinitely and eventually an upper limit is reached which corresponds to the experimentally measured density of C-S-H. To enable a mathematical description we assign C-S-H a concentration which varies between zero and C-S-H_{max} (see Table 1). Precipitation of C-S-H will therefore occur in regions where the solubility product is above its critical value and the concentration of C-S-H is below the maximum value, which gives

$$Q_2 = k_2 \mathrm{H}\left[[Ca^{2+}]^{1.5}[OH^-][H_2SiO_4^{2-}] - S_{eq}\right]\mathrm{H}[\,\text{C-S-H}_{max} - [\text{C-S-H}]\,], \tag{5}$$

where k_2 is a reaction rate constant with units of mol m^{-3} s^{-1} and H is the Heaviside function which takes the value zero for a negative argument and a value of unity for all other arguments.

Reactions (1) and (2) lead to an accumulation of calcium and hydroxide ions in solution, since they are produced in larger proportions than they are consumed. This process continues until the solution becomes supersaturated with respect to calcium hydroxide. At this point global precipitation of calcium hydroxide occurs. It has been suggested by Lota et al. [10] and Fujii and Kondo [20] that this triggers a large scale precipitation of C-S-H. This rapid increase in hydration products causes the cement to thicken and hence signifies the end of the induction period. Rather than incorporate the growth of calcium hydroxide into the model, we assume that the induction period ends when the concentration of calcium ions reaches this critical level.

It has been suggested by Pommersheim et al. [15] that the diffusivity of the ions will be reduced as the hydration shell builds up. We have included this feature in the model by assuming an expression for the diffusion coefficient of the form D_0g([C-S-H]), where D_0 is a typical ionic diffusivity in water, and the function g decreases monotonically from unity to ϵ as the concentration of C-S-H increases. The dimensionless parameter ϵ is chosen so that the diffusion coefficient varies over approximately one order of magnitude. We also assume that all the diffusion coefficients are equal. Experimental values for the diffusion coefficients of the ions in solution show this to be a reasonable assumption [21, p. 67].

Table 1 gives all the available experimental parameters. Unfortunately there seems to be no published information available on the reaction rate constants. Initially, we compute solutions using estimated values for the reaction rate constants which we later adjust to fit the experimental data.

3. Mathematical formulation

We feel that there is much to be learned from the study of the hydration of a single particle. To this end we propose a mathematical model for the hydration of a spherically symmetric grain of C_3S. The concentrations of the various chemical species a distance r from the centre of the grain a time t after mixing are

$$a(r,t) = [Ca^{2+}], \qquad b(r,t) = [OH^-],$$

$$c(r,t) = [H_2SiO_4^{2-}], \qquad d(r,t) = [\text{C-S-H}].$$

Table 1. Typical experimental parameters.

Model parameter	Experimental estimate
Typical diffusion coefficient (D_0)[a]	10^{-10} m^2 s^{-1}
Typical grain radius (R_0)[b]	10^{-5} m
Density of C_3S[b]	3120 kg m^{-3}
Maximum density of C-S-H (C-S-H_{max})	10^4 mol m^{-3}
Typical thickening time	2 hours
Equilibrium solubility product (S_{eq})	38 (mol m^{-3})$^{3.5}$

[a]Taken from Alberty and Silbey [21, p. 67]
[b]Taken from Taylor [22, Chapter 5]. The molar mass of C-S-H was taken to be 189g.
[c]Taken from Tzschichholz *et al.* [13].

We shall assume that R_0, the radius of the grain, is constant, even though the grain is losing mass via the dissolution of ions from its surface. This assumption can be justified by considering data given in [22, p. 150] which show that less than one percent of the C_3S is typically consumed during the induction period.

Equation (1) gives the boundary conditions at the grain surface as

$$-D_a \frac{\partial a}{\partial r}\bigg|_{r=R_0} = 3k_1, \quad -D_b \frac{\partial b}{\partial r}\bigg|_{r=R_0} = 4k_1, \quad -D_c \frac{\partial c}{\partial r}\bigg|_{r=R_0} = k_1, \tag{6}$$

where the diffusion coefficients are

$$D_a = D_b = D_c = D_0 \mathrm{g}(d). \tag{7}$$

To account for the effect of the other grains in the solution we apply no flux boundary conditions a distance r_b from the centre of the grain, which gives

$$\frac{\partial a}{\partial r}\bigg|_{r=r_b} = \frac{\partial b}{\partial r}\bigg|_{r=r_b} = \frac{\partial c}{\partial r}\bigg|_{r=r_b} = 0. \tag{8}$$

The parameter r_b determines the water cement ratio (w/c) of the mixture via

$$w/c = \frac{1}{\mu}\frac{r_b^3 - R_0^3}{R_0^3}, \tag{9}$$

where $\mu = 3{\cdot}12$ is the relative density of C_3S, which is included so that (9) gives the water cement ratio by mass. This allows us more easily to compare the predictions of the model with experimental data.

In the region outside the grain, $R_0 < r < r_b$, the concentrations of the four species obey the reaction-diffusion equations

$$\frac{\partial a}{\partial t} = \frac{1}{r^2}\frac{\partial}{\partial r}\left(D_a r^2 \frac{\partial a}{\partial r}\right) - \frac{3}{2}k_2 \mathrm{H}[a^{1.5}bc - S_{\mathrm{eq}}]\mathrm{H}[d_{\max} - d], \tag{10}$$

$$\frac{\partial b}{\partial t} = \frac{1}{r^2}\frac{\partial}{\partial r}\left(D_b r^2 \frac{\partial b}{\partial r}\right) - k_2 \mathrm{H}[a^{1.5}bc - S_{\mathrm{eq}}]\mathrm{H}[d_{\max} - d], \tag{11}$$

$$\frac{\partial c}{\partial t} = \frac{1}{r^2}\frac{\partial}{\partial r}\left(D_c r^2 \frac{\partial c}{\partial r}\right) - k_2 \mathrm{H}[a^{1.5}bc - S_{\mathrm{eq}}]\mathrm{H}[d_{\max} - d], \tag{12}$$

$$\frac{\partial d}{\partial t} = k_2 \mathrm{H}[a^{1.5}bc - S_{\mathrm{eq}}]\mathrm{H}[d_{\max} - d]. \tag{13}$$

Since all chemical concentrations are zero initially, the initial conditions are

$$a(r, 0) = b(r, 0) = c(r, 0) = d(r, 0) = 0. \tag{14}$$

Note that C-S-H, with concentration d, is immobile, so there is no diffusion in (13).

It is now convenient to define dimensionless concentrations

$$\alpha = \frac{1}{(S_{\mathrm{eq}})^{1/3\cdot 5}}a, \quad \beta = \frac{1}{(S_{\mathrm{eq}})^{1/3\cdot 5}}b, \quad \gamma = \frac{1}{(S_{\mathrm{eq}})^{1/3\cdot 5}}c, \quad \delta = \frac{1}{(S_{\mathrm{eq}})^{1/3\cdot 5}}d, \tag{15}$$

and the dimensionless length and time

$$\rho = \frac{r}{R_0}, \quad \tau = \frac{D_0}{R_0^2}t. \tag{16}$$

The dimensionless diffusion coefficient is

$$D = \frac{D_a}{D_0} = \frac{D_b}{D_0} = \frac{D_c}{D_0} = g(\delta). \tag{17}$$

In terms of these variables, (10), (11), (12) and (13) become

$$\frac{\partial \alpha}{\partial \tau} = \frac{1}{\rho^2}\frac{\partial}{\partial \rho}\left(D\rho^2 \frac{\partial \alpha}{\partial \rho}\right) - \frac{3}{2}\bar{k}_2 \mathrm{H}[\alpha^{1.5}\beta\gamma - 1]\mathrm{H}[\delta_{\max} - \delta], \tag{18}$$

$$\frac{\partial \beta}{\partial \tau} = \frac{1}{\rho^2}\frac{\partial}{\partial \rho}\left(D\rho^2 \frac{\partial \beta}{\partial \rho}\right) - \bar{k}_2 \mathrm{H}[\alpha^{1.5}\beta\gamma - 1]\mathrm{H}[\delta_{\max} - \delta], \tag{19}$$

$$\frac{\partial \gamma}{\partial \tau} = \frac{1}{\rho^2}\frac{\partial}{\partial \rho}\left(D\rho^2 \frac{\partial \gamma}{\partial \rho}\right) - \bar{k}_2 \mathrm{H}[\alpha^{1.5}\beta\gamma - 1]\mathrm{H}[\delta_{\max} - \delta], \tag{20}$$

$$\frac{\partial \delta}{\partial \tau} = \bar{k}_2 \mathrm{H}[\alpha^{1.5}\beta\gamma - 1]\mathrm{H}[\delta_{\max} - \delta], \tag{21}$$

and must be solved subject to the initial conditions,

$$\alpha(\rho, 0) = \beta(\rho, 0) = \gamma(\rho, 0) = \delta(\rho, 0) = 0, \tag{22}$$

and boundary conditions,

$$-D\frac{\partial \alpha}{\partial \rho}\bigg|_{\rho=1} = 3\bar{k}_1, \qquad \frac{\partial \alpha}{\partial \rho}\bigg|_{\rho=\rho_b} = 0, \tag{23}$$

$$-D\frac{\partial \beta}{\partial \rho}\bigg|_{\rho=1} = 4\bar{k}_1, \qquad \frac{\partial \beta}{\partial \rho}\bigg|_{\rho=\rho_b} = 0, \tag{24}$$

$$-D\frac{\partial \gamma}{\partial \rho}\bigg|_{\rho=1} = \bar{k}_1, \qquad \frac{\partial \gamma}{\partial \rho}\bigg|_{\rho=\rho_b} = 0. \tag{25}$$

The various dimensionless parameters are

$$\delta_{\max} = \frac{1}{(S_{\text{eq}})^{1/3\cdot 5}} d_{\max}, \quad \bar{k}_1 = \frac{k_1 R_0}{D_0 (S_{\text{eq}})^{1/3\cdot 5}}, \quad \bar{k}_2 = \frac{k_2 R_0^2}{D_0 (S_{\text{eq}})^{1/3\cdot 5}}, \tag{26}$$

and $\rho_b = r_b / R_0$, where the constant $\delta_{\max}$ represents the dimensionless maximum concentration, or experimentally measured density, of the C-S-H. Preliminary numerical investigations showed that a variation in the diffusion coefficient over one order of magnitude through the function $g(\delta)$ had no significant effect on the chemical concentrations in the bulk solution. We therefore used $D = 1$ in the results presented below.

4. Numerical method and results

An explicit finite difference scheme was used to compute solutions of (18), (19), (20) and (21). To reduce the overall number of points that were required, and thereby increase the computational efficiency of the scheme, we used the function

$$\Delta\rho_j = h \left[1 + 5 \left\{ 1 + \tanh \left(\rho_j - \frac{4\rho_b}{5} \right) \right\} \right], \tag{27}$$

to define the discrete set of points

$$\rho_0 = 1, \quad \rho_i = 1 + \sum_{j=1}^{i} \Delta\rho_j, \quad i = 1, 2 \ldots N, \tag{28}$$

at which we computed the chemical concentrations. This ensures that the majority of the grid points are close to the grain surface where the steepest gradients occur. To discretize the equations, we wrote all temporal derivatives as first order forward difference approximations and all spatial derivatives were replaced by three point central difference approximations. At $\rho = \rho_b$, the no flux boundary conditions were discretized using a two point formula and at $\rho = 1$ the constant flux boundary conditions were discretized using a three point formula. The time step was chosen so that $2\Delta\tau < (\Delta\rho)^2_{\min}$, where $(\Delta\rho)_{\min}$ is the minimum spatial step length. The values of $\Delta\rho_{\min}$ and $\Delta\tau$ that we used depended on the size of the domain but typically there were $N = 100$ grid points.

As discussed earlier no experimental values are available for k_1 and k_2 so it is necessary to estimate these values. The qualitative form of the results presented in this section are obtained if $k_2 \gg k_1$. We show later, by fitting our results to those of experiment, that this is the appropriate parameter range for the hydration reaction.

The initial numerical results used $k_1 = 10^{-5}$ mol m^{-2} s^{-1} and $k_2 = 1$ mol m^{-3} s^{-1}, which gives $\bar{k}_1 = 0{\cdot}35$ and $\bar{k}_2 = 0{\cdot}35$, and $\rho_b = 4$, which corresponds to a water cement ratio of about 20. To demonstrate the affect of imposing a limit on the C-S-H concentration we set C-S-H$_{\max} = 100$ mol m^{-3} which corresponds to a dimensionless concentration of approximately 35 mol m^{-3}. This enables the main features of the solution to be seen clearly.

Figures 1–4 show dimensionless concentration profiles for calcium ions, silica ions and C-S-H, respectively, at dimensionless times between $\tau = 40$ and $\tau = 600$. The horizontal axes show the scaled distance from the centre of the grain. The hydroxide ion concentration profiles display identical characteristics to those of the calcium ions and for brevity have been omitted. Although it is difficult to identify the concentrations at at particular time in Figures 3 and 4 the results have been displayed so that the overall structure of the solution can be visualised.

The calcium ion concentration decreases monotonically away from the grain surface, becomes almost uniform in the bulk solution, and increases linearly with time. Further numerical

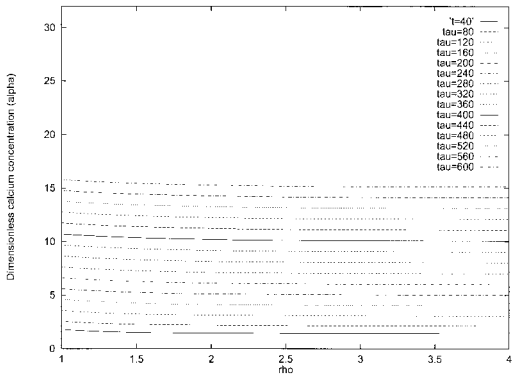

Figure 1. Calcium concentration with $\bar{k}_1 = 0{\cdot}35$, $\bar{k}_2 = 0{\cdot}35$ and C-S-H$_{\max} = 35$.

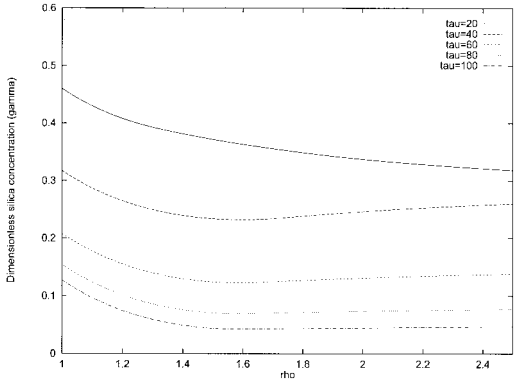

Figure 2. Early silica concentration with $\bar{k}_1 = 0{\cdot}35$, $\bar{k}_2 = 0{\cdot}35$ and C-S-H$_{\max} = 35$.

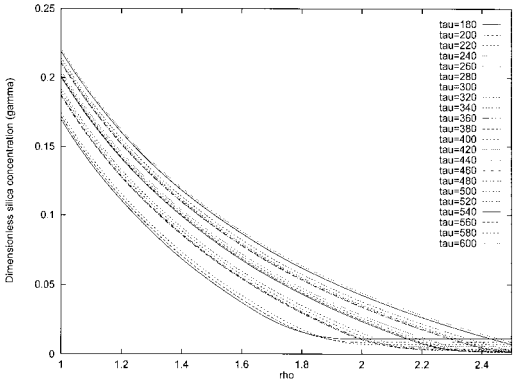

Figure 3. Silica concentration with $\bar{k}_1 = 0{\cdot}35$, $\bar{k}_2 = 0{\cdot}35$ and C-S-H$_{\max} = 35$.

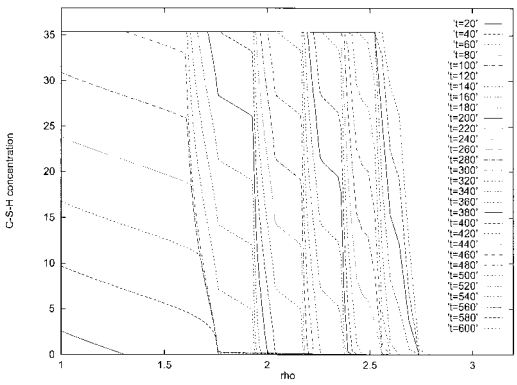

Figure 4. C-S-H concentration with $\bar{k}_1 = 0{\cdot}35$, $\bar{k}_2 = 0{\cdot}35$ and C-S-H$_{\max} = 35$.

investigation shows that identical behaviour is observed if there is no limit imposed on the C-S-H concentration and that the concentration in the bulk solution is unaffected by changing the parameter k_2.

Figure 4 shows C-S-H concentration profiles at different times. After an initial transient period, the first layer of C-S-H, or hydration shell, is observed to form within a region of constant width next to the grain surface. Once the maximum concentration is reached the system goes through another short transient period and then a new hydration shell forms, again in a region of fixed width. This process is repeated and successively thinner hydration shells are formed. We define the *reaction zone* to be the region in which the solubility product is above its equilibrium value and the C-S-H concentration is below its maximum value. C-S-H will only be deposited within the current reaction zone. Figure 4 shows that the reaction zone moves by discrete amounts away from the grain surface every time the C-S-H concentration reaches its maximum value.

The evolution of the silica ions has been illustrated on two separate plots. Figure 2 shows the early silica concentration, before the C-S-H concentration reaches its maximum value. After an initial growth in concentration, a spatial concentration profile forms which later decays with time at a decreasing rate. We note that if no maximum value is imposed on the C-S-H, the silica concentration tends to a steady state solution for $\tau \gg 1$. This corresponds to an equilibrium state where, to a first approximation, the amount of silica being consumed is equal to that being produced and a linear growth in C-S-H concentration is observed in region of fixed width. A typical solution when a maximum value is imposed on the C-S-H, is shown in Figure 3. The solution has a banded structure, with each band corresponding to the addition of another layer of C-S-H, or hydration shell. This indicates that the silica ion concentration is approximately constant during the formation of each of the hydration shells. As successive hydration shells are formed, the decay of the silica concentration takes place over a longer length scale and the concentration at the surface of the grain increases. This is because silica is only being consumed within the current reaction zone. Although it has not been illustrated, the concentration of silica at the edge of the domain decreases monotonically with time. Further investigations, using a different numerical solution method, suggest that the same features are observed when the movement of the grain boundary is included in the model.

In order to explain these features of the solution, note that there is a constant flux of ions from the surface of the grain in the ratio 3:4:1, calcium:hydroxide:silica. After a short period of time the solubility product reaches its equilibrium value at the grain surface and C-S-H starts to form. The system goes through a transient period, at the end of which the first hydration shell starts to form. When $\tau \approx 110$, the C-S-H reaches its maximum concentration at the grain surface and the system goes through another transient period after which another hydration shell forms, and the process repeats itself. Ions are consumed within the reaction zone in the ratio 1·5:1:1, calcium:hydroxide:silica. This leads to an increase in the concentration of calcium and hydroxide ions while the system tends to an equilibrium state in which the silica concentration does not change with time.

Further numerical investigation shows that the width of the hydration shells is a function of k_1/k_2. This can be explained by considering a reaction zone which moves by a discrete amount every time the C-S-H reaches its maximum value. After a layer of C-S-H is deposited the ions must diffuse through it before they can react. The ratio of production to consumption of ions is controlled by the ratio k_1/k_2. If k_1/k_2 is small, the ions are consumed rapidly, which leads to a thin reaction zone. This physical argument is shown to be correct by the asymptotic analysis given in Section 5.

We can now consider the effect of the water cement ratio on the ionic concentrations. We use the slightly different parameter values $k_1 = 10^{-5}$ mol m^{-2} s^{-1}, $k_2 = 20$ mol m^{-3} s^{-1} and C-S-H$_{\max} = 10^4$ mol m^{-3}. As we shall see later, these are close to the experimentally determined values, but k_2 is actually rather larger than this. However, our numerical method is unable to resolve the hydration shells if k_2 is made any larger. The qualitative features of the solution are as before.

Figures 5 and 6 show the concentration of the calcium and silica ions at the edge of the domain, $\rho = \rho_b$, for water cement ratios 5, 10 and 20.

The results show an increase in calcium ion concentration as the w/c ratio is decreased. The peak in the silica concentration represents the time at which precipitation of C-S-H begins. After this time, the silica ion concentration decreases as the w/c ratio decreases. These trends have been found experimentally [20], [23] A decrease in the w/c ratio produces larger ionic

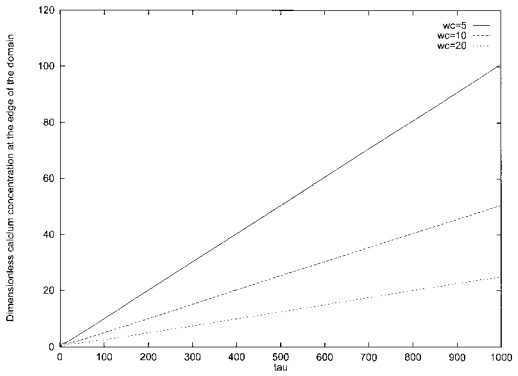

Figure 5. Calcium concentration at $\rho = \rho_b$ for different water cement ratios.

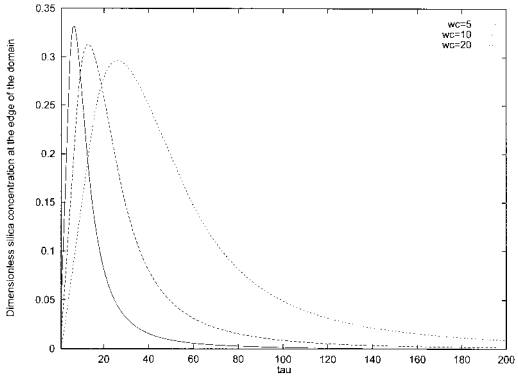

Figure 6. Silica concentration at $\rho = \rho_b$ for different water cement ratios.

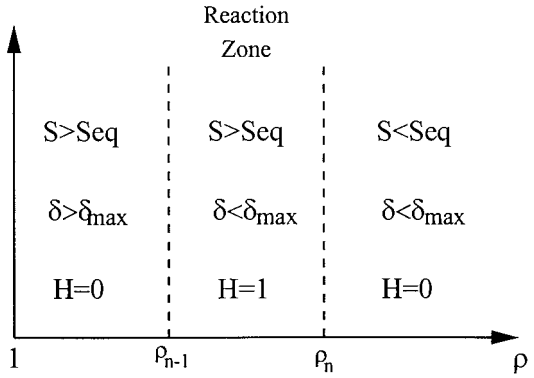

Figure 7. Schematic diagram of hydration shell formation.

concentrations as there is the same amount of chemical in a smaller volume, as can be seen for the calcium ion concentration. The silica ion concentration decreases because the large calcium ion concentration forces the precipitation reaction to proceed more rapidly and hence consume more silica from solution.

Having determined the qualitative form of the solution, we must now compare the results with those of experiments and estimate more appropriate values for the rate constants k_1 and k_2. We can do this by constructing an asymptotic solution.

5. Asymptotic solution

We assume a three region structure in which the current reaction zone is the central region. The nth reaction zone is $\rho_{n-1} \leq \rho \leq \rho_n$, as shown schematically in Figure 7. Behind the reaction zone ($\rho < \rho_{n-1}$) the C-S-H concentration is above its maximum value and ahead of the reaction zone ($\rho > \rho_n$) the solubility product is below its equilibrium value. Precipitation of hydration products therefore only occurs in the reaction zone. Numerical solutions have shown that during the addition of each layer of C-S-H the silica concentration is, to a good approximation, independent of time. We therefore assume that the silica concentration, γ, is a function of ρ only, at leading order. For $\rho_{n-1} \leq \rho \leq \rho_n$, γ satisfies

$$\frac{\partial \gamma}{\partial \tau} = \frac{1}{\rho^2}\frac{\partial}{\partial \rho}\left(\rho^2 \frac{\partial \gamma}{\partial \rho}\right) - \bar{k}_2 = 0, \tag{29}$$

subject to continuity conditions at $\rho = \rho_{n-1}$ and ρ_n which are obtained by solving the diffusion equation in the other two regions. At the surface of the grain, $\rho = 1$,

$$\frac{\partial \gamma}{\partial \rho} = -\bar{k}_1, \tag{30}$$

and at $\rho = \rho_b$

$$\frac{\partial \gamma}{\partial \rho} = 0. \tag{31}$$

The solutions in the three regions are

$$\gamma(\rho) = \begin{cases} \dfrac{\bar{k}_1}{\rho} + C_1 & \rho < \rho_{n-1} \\ \dfrac{\bar{k}_2 \rho^2}{6} + \dfrac{C_2}{\rho} + C_3 & \rho_{n-1} \le \rho \le \rho_n \\ C_4 & \rho > \rho_n, \end{cases} \tag{32}$$

where the constants C_1, C_2, C_3 and C_4 can be fixed in terms of each other by continuity of γ and $\partial\gamma/\partial\rho$ at $\rho = \rho_{n-1}$ and $\rho = \rho_n$. This also leads to an expression for the position of the edge of the nth reaction zone,

$$\rho_n = \sqrt[3]{1 + \frac{3n\bar{k}_1}{\bar{k}_2}}. \tag{33}$$

It is clear from (33) that each successive layer of C-S-H will be thinner than the last. This reflects the spherical geometry of the problem. To produce each C-S-H layer the same quantity of ions is consumed. This means that the volume of each shell is the same, and hence will become successively thinner. Note that if $\bar{k}_2 \gg n\bar{k}_1$, the difference between successive shell thicknesses is approximately $\bar{k}_1/\bar{k}_2$, consistent with our numerical results.

The concentration α satisfies the diffusion equation in the two regions on either side of the reaction zone. Inside the reaction zone, $\rho_{n-1} \le \rho \le \rho_n$, it satisfies

$$\frac{\partial \alpha}{\partial \tau} = \frac{1}{\rho^2}\frac{\partial}{\partial \rho}\left(\rho^2 \frac{\partial \alpha}{\partial \rho}\right) - \frac{3\bar{k}_2}{2}. \tag{34}$$

The numerical solutions suggest that an appropriate expansion is

$$\alpha = \alpha_0 \tau + \bar{\alpha}(\rho) + o(1), \tag{35}$$

and solving in each of the different regions subject to the appropriate boundary conditions gives,

$$\alpha(\rho, \tau) = \begin{cases} \alpha_0\tau + \dfrac{\alpha_0\rho^2}{6} + \dfrac{(\alpha_0 + 9\bar{k}_1)}{3\rho} + A_1 & 1 \le \rho < \rho_{n-1} \\ \alpha_0\tau + \dfrac{(\alpha_0 + 3\bar{k}_2/2)}{6} + \dfrac{A_2}{\rho} + A_3 & \rho_{n-1} \le \rho \le \rho_n \\ \alpha_0\tau + \dfrac{\alpha_0\rho^2}{6} + \dfrac{\alpha_0\rho_b^3}{3\rho} + A_4 & \rho_n < \rho \le \rho_b. \end{cases} \tag{36}$$

Table 2. Comparison of the asymptotic and numerical values for the growth rate of calcium ions in solution with $\bar{k}_1 = 0{\cdot}35$ and $w/c = 5, 10, 15$.

w/c ratio	5	10	20
Numerical growth rate	0·101	0·051	0·025
Asymptotic prediction	0·102	0·051	0·026

The continuity conditions at $\rho = \rho_{n-1}$ and $\rho = \rho_n$ fix the constants A_1, A_2, A_3 and A_4 along with the growth rate of calcium ions,

$$\alpha_0 = \frac{9\bar{k}_1}{2\mu w/c}. \tag{37}$$

The hydroxide ion concentration is found to grow at twice the rate of the calcium ions. Table 2 compares the prediction made by Equation (37) with the numerical results given in Figure 5 for different w/c ratios and shows that there is good agreement. Although we omit the details, it is also straightforward to determine the concentration of C-S-H, which is equal to C-S-H_{max} for $1 \leq \rho \leq \rho_{n-1}$, grows linearly with time within the reaction zone, and is an undetermined function of ρ for $\rho_n \leq \rho \leq \rho_b$.

We conclude this section with a discussion of the parameters that control the time for the calcium concentration to reach a given value and thus control the length of the induction period. In terms of dimensional variables, (37) shows that the induction period ends when $t = t_s$, where

$$t_s = \frac{2a_s\mu}{9}\frac{R_0 w/c}{k_1}, \tag{38}$$

and a_s is the concentration of calcium ions at the point of supersaturation with respect to calcium hydroxide formation. The length of the induction period is therefore proportional to a typical grain radius and the water cement ratio and inversely proportional to the rate constant k_1, which controls the flux of ions from the surface of the grain. In the cement industry the particle size distribution of a cement sample is normally given as a surface area. Our model predicts that the thickening time will be proportional to the square root of the surface area measurement.

6. Comparison with experimental data

We have now predicted a linear growth of calcium ion concentration in the pore solution once C-S-H precipitation has started. Experimental measurements [19], [20], [23] show that during a typical hydration reaction slightly different behaviour is observed. Initially there is a rapid increase in calcium ion concentration. This slows after a short period of time and a linear growth of calcium ions is then observed, in line with the predictions of our model. This has been explained by Taylor [24] in terms of the reaction rate of the surface reaction (1). The rate of this reaction is believed to be dependent on the amount of precipitated C-S-H at the grain surface. Reaction rate arguments of this type form the basis for protective coating theory models which were discussed in Section 1.

To incorporate this feature into our model we modify the surface reaction rate so that

$$Q_1 = 8k_1\left[\zeta - \frac{\mathrm{d}(R_0, t)(\zeta - 1)}{\mathrm{d}_{\max}}\right], \tag{39}$$

where the constant ζ is greater than unity. Expression (39) describes a flux which decreases from $Q_1 = 8\zeta k_1$ when no C-S-H has precipitated to $Q_1 = 8k_1$ as the first layer of C-S-H is deposited and builds up to its maximum concentration. This modified reaction rate was used to compute the ionic concentrations during the formation of the first hydration shell and the asymptotic prediction used to obtain the final linear growth rate.

We determined a value for k_1 by considering the final linear growth of calcium ions. The experimental results of Brown et al. [23] show that, after the first minute, the calcium concentration increases by approximately 0·5 mol m^{-3} per minute in a reaction with $w/c = 10$. Using this data in (38) shows that $k_1 = 1{\cdot}18 \times 10^{-5}$ mol m^{-2} s^{-1}, which gives $\bar{k}_1 = 0{\cdot}0206$.

To fix the constant k_2, we used data relating to the initial flux of ions into solution, and assumed that the calcium ion concentration increased linearly once the initial hydration shell had formed. This means that the concentration of C-S-H grows linearly at the surface of the grain. If we can determine from experimental data the time Δt between the first precipitation of C-S-H and the end of the formation of the first hydration shell, we can find k_2 using

$$k_2 = \frac{\mathrm{d}_{\max}}{\Delta t}. \tag{40}$$

The results of Brown et al. [23] show that $\Delta\tau \approx 45$ seconds, which gives $k_2 = 222$ mol m^{-3} s^{-1} and hence $\bar{k}_2 = 75{\cdot}6$.

We obtained an estimate of ζ, which controls the initial flux of ions from the surface of the grain, using an iterative method. Initially we computed the calcium ion concentration at $t = 60$ seconds using two initial estimates for ζ. We then compared these values with the experimental value [23] of 6 mol m^{-3} and used a bisection method to obtain a more accurate estimate for ζ. Using the experimental data of Brown et al. [23] we found that $\zeta \approx 21{\cdot}8$ for a w/c ratio of 10. The surface reaction therefore slows by a factor of approximately 22 as the initial hydration shell builds up.

Asymptotic result (33) can be used to obtain an estimate of the thickness of a typical layer of C-S-H. Using the above values of $\bar{k}_1$ and $\bar{k}_2$

$$\rho_n - \rho_{n-1} \approx \frac{\bar{k}_1}{\bar{k}_2} \approx 3 \times 10^{-4}. \tag{41}$$

This length is too small to be resolved using our finite difference scheme, so we had to modify it. This was done by assuming that the thickness of the first hydration shell is asymptotically small. We can then incorporate the consumption of ions within the shell into the boundary condition at $\rho = 1$. The modified boundary conditions at the grain surface are

$$\left.\frac{\partial\alpha}{\partial\rho}\right|_{\rho=1} = -\left[3\bar{k}_1 - \frac{3}{2}\bar{k}_2\rho^*\right], \tag{42}$$

$$\left.\frac{\partial\beta}{\partial\rho}\right|_{\rho=1} = -\left[4\bar{k}_1 - \bar{k}_2\rho^*\right], \tag{43}$$

$$\left.\frac{\partial\gamma}{\partial\rho}\right|_{\rho=1} = -\left[\bar{k}_1 - \bar{k}_2\rho^*\right], \tag{44}$$

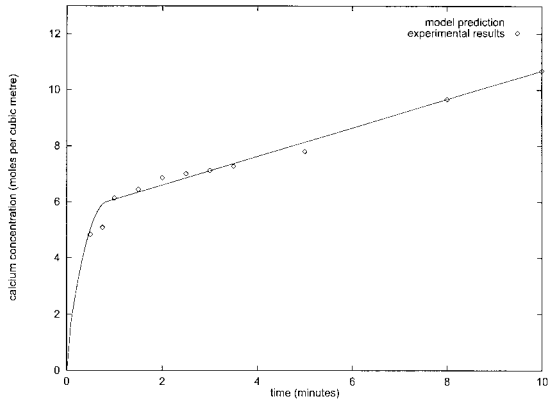

Figure 8. Comparison of experimental results with the model predictions for the hydration of a C_3S paste with $w/c = 10$.

where the asymptotic prediction of the shell width, ρ^*, as calculated in the previous section, is

$$\rho^* = \begin{cases} 0 & t < t_0 \\ \sqrt[3]{1 + \dfrac{3Q_1}{\bar{k}_2}} - 1 & t \geq t_0, \end{cases} \tag{45}$$

where t_0 is the time at which C-S-H begins to precipitate. The second terms on the right hand sides of (42), (43) and (44) are zero when $t < t_0$, and when $t > t_0$ account for the consumption of ions which occurs during the formation of the first hydration shell. Note that we obtained the value of ρ^* by assuming a constant silica concentration during the addition of the first layer of C-S-H. This means that, although our modified scheme is able to predict the calcium concentration, it predicts a constant silica concentration for $t > t_0$.

Figure 8 shows a comparison between the model predictions and the experimental data of Brown et al. [23] for a hydrating C_3S paste with $w/c = 10$. The method described above was used to obtain the calcium concentration during the first minute of hydration. The final linear growth at the edge of the domain was then obtained using (38). The model predictions agree well with the experimental data.

During experiments, the linear growth continues until the solution is supersaturated with respect to calcium hydroxide. This normally occurs after about 2 hours once the calcium concentration reaches approximately 45 mol m^{-3}. Since each shell takes 45 s to form, 160 shells will have been formed after 2 h. Using (33) we find that the thickness of the complete hydration shell at the end of the induction period is approximately 4·2% of the initial grain radius, in reasonable agreement with experiment.

7. Conclusion

Using the fundamental laws of mass transport and basic cement reaction kinetics, we have formulated a mathematical model for the microstructural evolution of cement and solved the resulting equations. The solutions suggest that successive layers of tricalcium silicate build up on the surface of a spherically symmetric grain of tricalcium silicate and form a hydration

shell. We have obtained predictions of calcium and silica ion concentrations that agree qualitatively with experimental data. Using asymptotic methods, we have found an approximate analytical expression for the growth rate of the concentration of calcium ions in solution. We have thereby determined the factors that control the thickening time of cement. We have also been able to determine the kinetic rate constants from experimental data and, after a modification to the kinetic scheme, make predictions that agree with experimental results.

The results of our model suggest that the driving mechanism during the initial stages of cement hydration is a combination of a delayed nucleation and a protective coating mechanism. The results of Damiot et al. [24] show the kinetics of tricalcium silicate hydration to be strongly dependent on the water cement ratio. Thus although the model results do not support the osmotic theory of hydration it could be that this description is valid for different water cement ratios.

Acknowledgements

The authors would like to acknowledge the financial support of Rugby Cement, and many helpful conversations with Arthur Harrision and John Bensted.

References

1. J. D. Birchall, A. J. Howard and J. E. Bailey. On the Hydration of Portland Cement. *Proc. R. Soc. London* 360 (1978) 445–453.
2. D. D. Double. New developments in understanding the chemistry of cement hydration. *Phil. Trans. R. Soc. London* A310 (1983) 53–66.
3. P. Meredith, A. M. Donald and K. Luke. Pre-induction and induction hydration of tricalcium silicate: An environmental scanning electron microscope study. *J. Mat. Sci.* 30 (1995) 1921–1930.
4. H. N. Stein and J. M. Stevels. Influence of silica on the hydration of 3 CaO,SiO_2. *J. Appl. Chem.* 14 (1964) 338–345.
5. J. G. de Jong and H. N. Stein, and J. M. Stevels. Hydration of tricalcium silicate. *J. Appl. Chem.* 17 (1967) 246–250.
6. T. C. Powers. Einige physikalische Gesichtspunkte zur Hydratation von Portlandzement. *Zement-Kalk-Gips* 14 (1961) 81–87.
7. D. D. Double, A. Hellawell and S. J. Perry. The hydration of Portland cement. *Proc. R. Soc. London* A369 (1978) 435–451.
8. D. D. Lasic, M. M. Pintar and R. Blinc. Are proton NMR observations supportive of the osmotic model of cement hydration?. *Phil. Mag. Lett.* 58 (1988) 227–232.
9. L. D. Mitchelle, M. Prica and J. D. Birchall. Aspects of Portland cement hydration studied using atomic force microscopy. *J. Mat. Sci.* 31 (1996) 4207–4212.
10. J. S. Lota, J. Bensted, J. Munn and P. L. Pratt. Hydration of class G oilwell cement at 20 °C and 5 °C. *L'industria italiana del Cemento* 725 (1997) 776–798.
11. D. Damidot and A. Nonat. Hydration of C_3S. In: A. Nonat and J. C. Mutin, (eds), *Hydration and Setting of Cements*. London: E & F Spon (1992) 23–34.
12. D. Bentz, E. J.Garboczi, M. F. Kleyn and P. E.Stuzman. Cellular automaton simulations of cement hydration and microstructural development. *Modelling Simul. Mater. Sci. Eng.* 2 (1994) 783–808.
13. F. Tzschichholz, H. J. Herrmann and H. Zanni. Reaction-diffusion model for the hydration and setting of cement. *Phys. Rev.*, E53 (1996) 2629–2637.
14. R. Kondo and S. Ueda. Kinetics and mechanisms of the hydration of cements. In *Proc. Int. Conf. Chem. Cem.*. Toyko (1968) 102–108.
15. J. M. Pommersheim and J. R. Clifton. Mathematical modelling of tricalcium silicate hydration. *Cem. Conc. Res.* 9 (1979) 765–770.
16. J. M. Pommersheim, J. R. Clifton. and G. J. Frohnsdorff. Mathematical modelling of tricalcium silicate hydration. II. Hydration sub-models and the effect of model parameters. *Cem. Conc. Res.* 12 (1982) 765–772.

17. P. Barret and, D. Bertrandie. Fundamental hydration kinetic features of the major cement constituents - Ca_3SiO_5 and β-Ca_2SiO_4. *J. Chim. Phys.* 82 (1986) 765–775.
18. S. A. Greenberg, T. N. Chang and E. Anderson. Investigation of colloidal hydrated calcium silicates. I. Solubility products. *J. Phys. Chem.* 64 (1960) 1151–1157.
19. N. L. Thomas and D. D. Double. Calcium and silicon concentrations in solution during the early stages of hydration of portland cement and tricalcium silicate. *Cem. Conc. Res.* 11 (1981) 675–687.
20. K. Fujii, and M. Kondo. Hydration of tricalcium silicate in a very early stage. In: *Proc. Int. Conf. Chem. Cem.*. Toyko (1968) 206–212.
21. R. A. Alberty and R. J. Silbey. *Physical Chemistry*. New York: Wiley and Sons (1992) 898 p.
22. H. F. W. Taylor. *Cement Chemistry*. London: Academic Press (1997) 499 p.
23. P. W. Brown, J. M. Pommersheim and G. J. Frohnsdorff. A kinetic model for the hydration of tricalcium silicate. *Cem. Conc. Res* 15 (1985) 35–41.
24. D. Damidot, A. Nonat and P. Barret. Kinetics of tricalcium silicate hydration in diluted suspensions by microcalorimetric measurements. *J. Am. Ceram. Soc.* 73 (1990) 3319–3322.